Experimental Implementation of the Optimal Linear-Optical Controlled Phase Gate

Karel Lemr,[1] A. Černoch,[1] J. Soubusta,[1] K. Kieling,[2] J. Eisert,[2,3] and M. Dušek[4]

[1]*Joint Laboratory of Optics of Palacký University and Institute of Physics of Academy of Sciences of the Czech Republic, 779 07 Olomouc, Czech Republic*

[2]*Institute of Physics and Astronomy, University of Potsdam, 14476 Potsdam, Germany*

[3]*Institute for Advanced Study Berlin, 14193 Berlin, Germany*

[4]*Department of Optics, Faculty of Science, Palacký University, 771 46 Olomouc, Czech Republic*

(Received 26 July 2010; published 6 January 2011)

We report on the first experimental realization of optimal linear-optical controlled phase gates for arbitrary phases. The realized scheme is entirely flexible in that the phase shift can be tuned to any given value. All such controlled phase gates are optimal in the sense that they operate at the maximum possible success probabilities that are achievable within the framework of postselected linear-optical implementations with vacuum ancillas. The quantum gate is implemented by using bulk optical elements and polarization encoding of qubit states. We have experimentally explored the remarkable observation that the optimum success probability is not monotone in the phase.

DOI: 10.1103/PhysRevLett.106.013602 PACS numbers: 42.50.Ex, 03.67.Lx

Linear-optical architectures belong to the most prominent platforms for realizing protocols of quantum information processing [1,2]. In small-scale applications of quantum information, such as in quantum repeaters, they will quite certainly play a key role. Unsurprisingly, significant research effort has been dedicated in recent years to experimental realization of universal linear-optical quantum gates. Linear-optical quantum gates are probabilistic by their very nature [1]. Therefore, the exact trade-offs between properties of a gate, such as entangling power, and its probability of success are in the focus of attention.

We explore this trade-off for the first time experimentally. We present data from an experimental realization of a linear-optical, postselected controlled phase gate implementing the following operation on two qubits:

$$|j, k\rangle \mapsto u_{j,k}|j, k\rangle, \qquad j, k = 0, 1, \tag{1}$$

where $u_{1,1} = e^{i\phi}$ and $u_{0,0} = u_{0,1} = u_{1,0} = 1$. It is key to this experiment that this angle can be chosen in a fully tunable fashion, hence adding a flexible scheme to the linear-optical quantum-information-processing toolbox.

Controlled phase gates are important members of this toolbox. For example, they play a key role in the circuit for quantum Fourier transform [3] or quantum simulation tasks [4]. They are entangling quantum gates, in general, and, together with single-qubit operations, they form sets of universal gates for quantum computing. Notice that the controlled-NOT gate can be obtained by applying a Hadamard transform to the target qubit before and after a controlled phase gate with phase shift π. What is more, nonmaximally entangled states can be used in the nonlocal implementation of controlled phase gates [5].

Previous experimental work was devoted to the linear-optical realization of a special case of the controlled phase gate with the fixed phase $\varphi = \pi$ [6]. Reference [7] presents an experiment with phases different from π but with a nonoptimal probability of success. The optimal success probability has recently been identified theoretically in Ref. [8]. This optimum probability we have indeed reached in the experiment described in this Letter. We observe the quite remarkable trade-off between the phase shift applied by the gate and its success probability, which is—surprisingly—not monotonous in the phase on $[0, \pi]$. The success probability decreases rapidly for small phases but remains almost constant for phases between $\pi/4$ and π. This experiment is hence expected to be interesting both conceptually as well as technologically, since a fully tunable bulk linear-optical architecture is presented, uplifting tunable schemes for quantum state preparation [9] to the level of quantum information processing.

Theoretical framework.—For postselected linear-optical gates, the beam splitter matrix A describing a general linear optics network is constrained by the action of the gate (1) as $\mathrm{per}A[c_i, c_j|c_k, c_l] = u_{i,j}\delta_{i,k}\delta_{j,l}$, where $i, j, k, l = 0, 1$. The left-hand side is the permanent of a matrix filled by matrix elements of A [10]. $c_0 = (0, 1)$ and $c_1 = (1, 0)$ are vectors describing the usual dual-rail encoding into Fock states on two modes [11]. Because of postselection, only outcomes in the computational subspace $\mathrm{span}\{|c_k, c_l\rangle\}$ are considered, giving rise to 16 quadratic equations in $A_{m,n}$. The solutions are all of the form $A = 1_2 \oplus B$, where two modes are bypassed and B describes the interaction of the two logical-1 modes. This amounts to a balanced Mach-Zehnder interferometer inside of which phase shifts $\phi_\pm$ are applied to both modes and one mode's amplitude is damped by a factor of θ. It turns out [8] that for $\varphi \in [0, \pi]$ the optimal success probability takes the form

$$p_s(\varphi) = \left(1 + 2\left|\sin\frac{\varphi}{2}\right| + 2^{3/2}\sin\frac{\pi - \varphi}{4}\left|\sin\frac{\varphi}{2}\right|^{1/2}\right)^{-2},$$

 © 2011 The American Physical Society

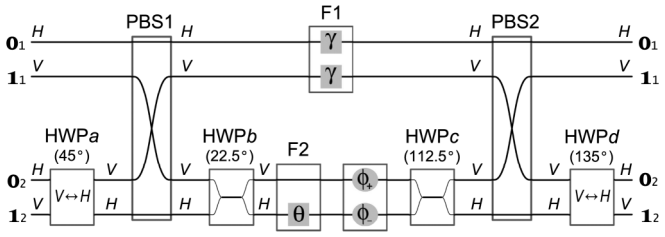

FIG. 1. Conceptual scheme of the gate. Vertically (V) and horizontally (H) polarized components of the same beam are drawn separately for clarity. In polarization beam splitters PBS1 and PBS2 the vertical components are reflected. Half-wave plates HWPb and HWPc act as "beam splitters" for V and H polarization modes. F1 and F2 are filters (attenuators); F1 acts on the both polarization modes, F2 on the H component only. Phase shifts ϕ_+ and ϕ_- are introduced by proper path differences in the respective modes. HWPa and HWPd just swap vertical and horizontal polarizations. In the final setup they are omitted for simplicity, and the second qubit is encoded inversely with respect to the first qubit.

and the phases in the inner Mach-Zehnder interferometer (between HWPb and HWPc; see Fig. 1) are defined by

$$\cot\phi_\pm = \cot\frac{\varphi+\pi}{4} \pm \left((2-2\cos\varphi)^{1/4}\sin\frac{\varphi+\pi}{4}\right)^{-1},$$

and the damping of one arm is done by an attenuator (neutral-density filter) with an amplitude transmissivity of

$$\theta = \left(\frac{1+2\sin\frac{\varphi}{2}-2(2-2\cos\varphi)^{1/4}\cos\frac{\varphi+\pi}{4}}{1+2\sin\frac{\varphi}{2}+2(2-2\cos\varphi)^{1/4}\cos\frac{\varphi+\pi}{4}}\right)^{1/2}.$$

The two attenuators with amplitude transmissivity $\gamma = p_s^{1/4}$ in the upper beams are used to damp the amplitude of the bypassed modes to compensate for the overall losses in the lower beams.

Details of the experiment.—As the starting point of this experiment we generate a pair of photons in the process of type-I spontaneous parametric down-conversion. The laser beam of 250 mW of cw optical power emitted by a krypton-ion laser at 413 nm impinges on the $LiIO_3$ crystal. Pairs of photons at 826 nm are collected by using single mode fibers serving also as spatial filters. Subsequently, polarization controllers are employed to adjust the horizontal polarization of the photons.

The half-wave plates (HWPs) and quarter-wave plates (QWPs) in the input arms (see Fig. 2) are used to set the input states. Subsequently, the photons are superposed on the first polarizing beam splitter PBS1 which transmits horizontal and reflects vertical polarization. Because of imperfections, the transmissivity for horizontal polarization is only 95% (the remaining 5% are reflected). Polarization beam splitters also introduce parasitic phase shifts between vertical and horizontal polarization components. After leaving the PBS1, the photons in the upper arm are subjected to the action of half-wave plate HWP21.

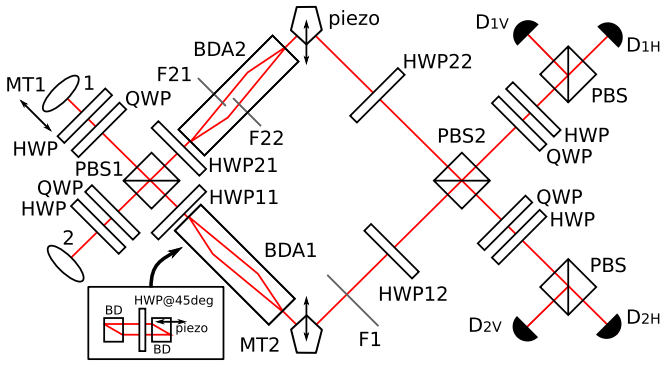

FIG. 2 (color online). Scheme of the actual experimental setup (see the text and Ref. [17] for details).

When set to 22.5° it performs the transformation $|H\rangle \mapsto (|H\rangle + |V\rangle)/\sqrt{2}$, $|V\rangle \mapsto (|H\rangle - |V\rangle)/\sqrt{2}$, where $|H\rangle$ and $|V\rangle$ denote horizontal and vertical polarization states, respectively. The lower arm is also equipped with a half-wave plate (HWP11), but it is set to zero (its presence just guarantees the same optical paths, dispersion effects, etc., in both arms). Behind the wave plates there are the beam-divider assemblies BDA1 and BDA2. They consist of two beam dividers (BD) splitting and subsequently rejoining horizontal and vertical polarizations. BDA2 is equipped with gradient neutral-density filters F21 and F22 (see Fig. 2). This way one can perform arbitrary polarization sensitive losses. BDA1 is used just to equilibrate the beam position and the optical length of both arms. It also avoids potential problems with different dispersion effects in the two arms. After leaving the beam-divider assemblies, the photons propagate through half-wave plates HWP12 and HWP22. HWP22 is set to 22.5°, reversing thus the transformation imposed by HWP21. HWP12 is set to 45° to compensate for the polarization flip between the H and V polarizations performed by BDA1. The lower arm is equipped with a gradient neutral-density filter F1 to apply polarization-independent losses. The gate operation itself is completed by overlapping the photons on the second polarizing beam splitter PBS2. To be able to perform complete state and thereby *process tomography*, we employ polarization analysis in both output arms. The analysis consists of QWPs and HWPs followed by polarizing beam splitters, cutoff filters, and single mode fibers leading to single photon detectors.

Gate operation.—The setup is then adjusted to perform the gate operation. First we set filters F21 and F1 to introduce the required losses. After that the wave plates HWP21 and HWP22 are set to 22.5°. The phase in the beam-divider assembly BDA2 is set to maximize the visibility of the interferometer formed by PBS1 and PBS2. The precise tuning of the gate is then performed by switching between the inputs $|H_1, R_2\rangle$ and $|V_1, R_2\rangle$, where indices 1 and 2 denote the input modes and R stands for the right circular polarization. Using the circular detection basis in the second output arm, we can observe the phase applied

by the gate when the polarization of the first input photon flips from $|H\rangle$ to $|V\rangle$. In this configuration we also tune the phase shift inside the beam-divider assembly BDA2 and the phase shift between the two arms of the Mach-Zehnder interferometer formed by PBS1 and PBS2.

Results.—Gradually we have adjusted the gate to apply 7 phases in the range between 0 and π. Each time, we have performed complete process tomography and estimated the process matrix by using the maximum likelihood method. Fidelities of the process lie in the range from 84% to 95% (see Table I). Figure 3 shows an example of an experimentally obtained process matrix and its theoretical counterparts for $\varphi = \pi/2$.

For each selected phase we simultaneously measured two-photon coincidence counts between detectors $D_{1H} + D_{2H}$, $D_{1V} + D_{2V}$, $D_{1H} + D_{2V}$, and $D_{1V} + D_{2H}$, each for 3×3 combinations of polarization measurement bases in the output arms. This amounts to measuring projections onto horizontal and vertical, diagonal $[|D\rangle = (|H\rangle + |V\rangle)/\sqrt{2}]$ and antidiagonal $[|A\rangle = (|H\rangle - |V\rangle)/\sqrt{2}]$, and right circular $[|R\rangle = (|H\rangle + i|V\rangle)/\sqrt{2}]$ and left circular $[|L\rangle = (|H\rangle - i|V\rangle)/\sqrt{2}]$ polarizations. The unequal detector efficiencies were compensated by proper rescaling of the measured coincidence counts [12]. Each measurement was done for 36 different input product states, namely, for 6×6 combinations of polarization state vectors $|H\rangle$, $|V\rangle$, $|D\rangle$, $|A\rangle$, $|R\rangle$, and $|L\rangle$ of each input photon. This complex measurement provided us with tomographically complete data enabling us to fully characterize the implemented operation by quantum process tomography [13,14] as well as to reconstruct density matrices of output states for each used input state.

Active stabilization.—Each setting of an input and output polarization basis was preceded by an active stabilization. For the purpose of the stabilization, the fixed input state and output detection basis were always used. In this setting the visibility in the interferometer formed by PBS1 and PBS2 was measured. If this visibility was lower than a selected threshold (usually 94%), then the positions of MT1 (two-photon temporal overlap) and MT2 (equilibration of interferometer arms) were optimized and the phase drift was compensated. Finally, the required polarizations were set and data were accumulated within 5 s.

TABLE I. Process fidelities (F_χ), average (F_{av}) and minimal (F_{min}) output-state fidelities, average ($\mathcal{P}_{\text{av}}$) and minimal ($\mathcal{P}_{\text{min}}$) output-state purities, and actually observed ($p_{s,\text{obs}}$) and theoretically predicted ($p_{s,\text{th}}$) success probabilities for different phases (φ). All values are expressed in percents.

φ	F_χ	F_{av}	F_{min}	$\mathcal{P}_{\text{av}}$	$\mathcal{P}_{\text{min}}$	$p_{s,\text{obs}}$	$p_{s,\text{th}}$
0	93.9	95.6	83.5	96.0	87.3	85.9 ± 1.3	100
0.05π	94.8	96.1	90.6	96.5	87.0	36.6 ± 0.8	34.8
0.125π	91.0	90.3	77.0	95.4	86.6	19.0 ± 0.5	21.0
0.25π	84.2	88.1	73.3	89.6	67.0	11.2 ± 0.3	13.3
0.5π	86.3	88.8	81.5	90.3	75.9	9.0 ± 0.2	9.0
0.75π	84.0	86.8	63.3	89.8	70.5	8.0 ± 0.2	8.8
π	83.5	85.6	71.0	92.2	82.7	12.0 ± 0.1	11.1

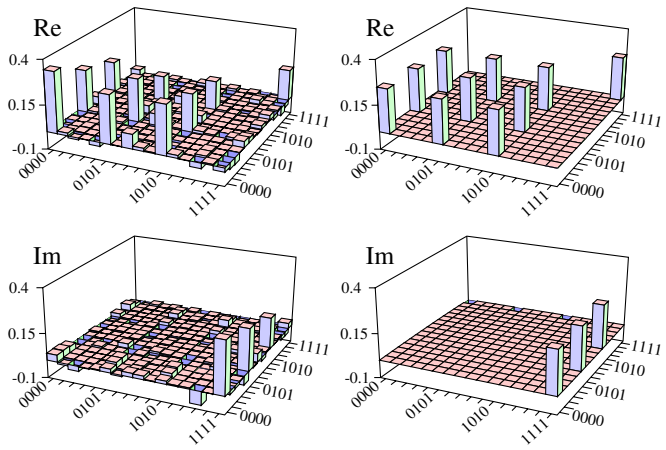

FIG. 3 (color online). Choi matrices for the gate with $\varphi = \pi/2$. The left top panel shows the real part of the reconstructed process matrix, while the left bottom one displays its imaginary part. The process fidelity $F_\chi = 86\%$. The two right panels show the ideal matrix.

Process tomography.—Any quantum operation can be fully described by a completely positive map and—according to the Jamiolkowski-Choi isomorphism—represented by a positive-semidefinite operator χ on the tensor product of input and output Hilbert spaces [15]. In our case, χ is a 16×16 square matrix. From the measured data we can reconstruct χ for any setting of φ by using maximum likelihood estimation [14,16]. To quantify the quality of the operation we calculate the process fidelity; if χ_{id} is a one-dimensional projector, its common definition is $F_\chi = \text{Tr}[\chi\chi_{\text{id}}]/(\text{Tr}[\chi]\text{Tr}[\chi_{\text{id}}])$. Here χ_{id} represents the ideal transformation corresponding to the controlled phase gate. Specifically, $\chi_{\text{id}} = \sum_{i,j,k,l=V,H} |i, j\rangle\langle k, l| \otimes U|i, j\rangle \times \langle k, l|U^\dagger$, where U stands for the unitary operator on two qubits defined by Eq. (1). We have also reconstructed the density matrices of output two-photon states corresponding to all product input states $|j, k\rangle$, $j, k \in \{H, V, D, A, R, L\}$. This was done for all values of φ. An important parameter characterizing the gate performance is the fidelity of output states ρ_{out} defined as $F = \langle\psi_{\text{out}}|\rho_{\text{out}}|\psi_{\text{out}}\rangle$, where $|\psi_{\text{out}}\rangle = U|\psi_{\text{in}}\rangle$ and $|\psi_{\text{in}}\rangle$ is the input state vector. Table I contains the average and minimal values of state fidelities for different phases. Fidelities F_{av} are averaged over all output states corresponding to our 36 input states; F_{min} denote minimal values. Another important characteristics is the purity of the output state ρ_{out}, defined as $\mathcal{P} = \text{Tr}[\rho_{\text{out}}^2]$. If the input state is pure, the output state is expected to be pure as well.

Trade-off in success probabilities.—The most important result of this Letter—aside from the technological implications—is the experimental verification of the trade-off between the phase shift applied by the gate and the

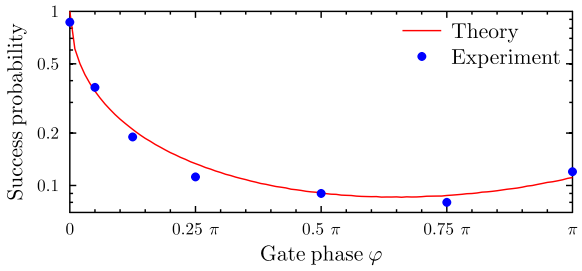

FIG. 4 (color online). Success probability of the gate.

corresponding success probability of the gate. We have estimated the success probability for each value of the selected phase shifts. It was calculated as a ratio of the number of successful gate operations per time interval and the number of reference counts during the same interval (measured with no filters and with the wave plates set to 0). We have determined the success probability for all selected input states. These probabilities were averaged and the standard deviations of the means were calculated. Notice that the calibration measurements collect coincidence counts behind the setup (by using the same detectors as in the subsequent measurements); thus, all the ''technological'' losses in the setup (about 60%) and low detector efficiencies are included in the calibration. Therefore, the estimated success probabilities are not burdened by these technological losses. They can be compared with the theoretical predictions in Table I and in Fig. 4. One can see a very good agreement with the theoretical prediction.

Conclusions.—We have built the first implementation of the tunable linear-optical controlled phase gate which is optimal for any value of the phase shift. Changing the parameters of the setup the gate can apply any phase shift from the interval $[0, \pi]$ on the controlled qubit. We have thoroughly tested the performance of the gate by using full quantum process tomography. Obtained process fidelities range from 84% to 95%. We have determined that the main limiting factors for the fidelities are imperfect two-photon spatial and temporal overlap and birefringence of PBS causing partial distinguishability between different polarization modes. We have also experimentally verified that all our controlled phase gates are optimal in the sense that they operate at the maximum possible success probabilities that are achievable by linear-optical setups. The experimental verification of this trade-off between the phase shift applied by the gate and the corresponding success probability of the gate is the most notable result of our work. It demonstrates the contraintuitive fact that the optimal success probability is not monotonous with the phase shift increasing from 0 to π. It is the hope that the flexible tool established here proves useful in devising further linear-optical circuits for quantum information processing and that ideas developed in this work find their way to realization in fully integrated optical architectures.

This work was supported by the Czech Ministry of Education (1M06002, MSM6198959213, and RCPTM - CZ.1.05/2.1.00/03.0058), the Czech Science Foundation (202/09/0747), the EU (QESSENCE, MINOS, and COMPAS), the EURYI, and Palacky University (PrF-2010-009 and PrF-2010-020).

[1] E. Knill *et al.*, Nature (London) **409**, 46 (2001).
[2] W. J. Munro *et al.*, J. Opt. B **7**, S135 (2005); J. L. O'Brien, Science **318**, 1567 (2007); I. A. Walmsley, Science **319**, 1211 (2008); M. Aspelmeyer and J. Eisert, Nature (London) **455**, 180 (2008); A. Politi *et al.*, Science **320**, 646 (2008); B. J. Smith *et al.*, Opt. Express **17**, 13 516 (2009).
[3] M. A. Nielsen and I. L. Chuang, *Quantum Computation and Quantum Information* (Cambridge University Press, Cambridge, England, 2000).
[4] B. Lanyon *et al.*, Nature Chem. **2**, 106 (2010).
[5] J. Eisert, K. Jacobs, P. Papadopoulos, and M. B. Plenio, Phys. Rev. A **62**, 052317 (2000); T. B. Pittman, M. J. Fitch, B. C. Jacobs, and J. D. Franson, *ibid.* **68**, 032316 (2003); J. I. Cirac, W. Dür, B. Kraus, and M. Lewenstein, Phys. Rev. Lett. **86**, 544 (2001).
[6] H. F. Hofmann and S. Takeuchi, Phys. Rev. A **66**, 024308 (2002); N. K. Langford *et al.*, Phys. Rev. Lett. **95**, 210504 (2005); N. Kiesel *et al.*, *ibid.* **95**, 210505 (2005).
[7] B. P. Lanyon *et al.*, Nature Phys. **5**, 134 (2009).
[8] K. Kieling, J. O'Brien, and J. Eisert, New J. Phys. **12**, 013003 (2010).
[9] W. Wieczorek *et al.*, Phys. Rev. Lett. **101**, 010503 (2008).
[10] S. Scheel, arXiv:quant-ph/0406127.
[11] K. Kieling, Ph.D. thesis, Imperial College London, 2008.
[12] J. Soubusta *et al.*, Phys. Rev. A **76**, 042318 (2007).
[13] J. F. Poyatos, J. I. Cirac, and P. Zoller, Phys. Rev. Lett. **78**, 390 (1997); I. L. Chuang and M. A. Nielsen, J. Mod. Opt. **44**, 2455 (1997); J. Fiurášek and Z. Hradil, Phys. Rev. A **63**, 020101 (2001); M. F. Sacchi, *ibid.* **63**, 054104 (2001).
[14] M. Ježek, J. Fiurasek, and Z. Hradil, Phys. Rev. A **68**, 012305 (2003).
[15] A. Jamiołkowski, Rep. Math. Phys. **3**, 275 (1972); M.-D. Choi, Linear Algebra Appl. **10**, 285 (1975).
[16] *Quantum State Estimation*, edited by M. G. A. Paris and J. Řeháček, Lect. Notes Phys. Vol. 649 (Springer, Berlin, 2004).
[17] See supplementary material at http://link.aps.org/supplemental/10.1103/PhysRevLett.106.013602 for more detailed information on technical aspects of the experimental setup.